



Providing Choice & Value

Generic CT and MRI Contrast Agents



CONTACT REP

AJNR

This information is current as
of July 18, 2025.







**Diagnostic Value of Multiparameter
MRI-Based Radiomics in Pediatric Myelin
Oligodendrocyte Glycoprotein Antibody–
Associated Disorders**

Ting Li, Xin Chen, Yang Jing, Haoru Wang, Ting Zhang, Li
Zhang, Hao Ding, Mingye Xie and Ling He

AJNR Am J Neuroradiol published online 16 November
2023

<http://www.ajnr.org/content/early/2023/11/16/ajnr.A8045>

Diagnostic Value of Multiparameter MRI-Based Radiomics in Pediatric Myelin Oligodendrocyte Glycoprotein Antibody–Associated Disorders

 Ting Li,  Xin Chen,  Yang Jing,  Haoru Wang, Ting Zhang, Li Zhang, Hao Ding,  Mingye Xie, and  Ling He



ABSTRACT

BACKGROUND AND PURPOSE: Myelin oligodendrocyte glycoprotein antibody-associated disorders (MOGAD) have a higher prevalence among children. For children undergoing the initial manifestation of MOGAD, prompt diagnosis has paramount importance. This study assessed the performance of multiparameter MRI-based radiomics in distinguishing patients with and without MOGAD with idiopathic inflammatory demyelinating diseases.

MATERIALS AND METHODS: We enrolled a cohort of 121 patients diagnosed with idiopathic inflammatory demyelinating diseases, including 68 children with MOGAD and 53 children without MOGAD. Radiomics models (TIWI, T2WI, FLAIR, and compound model) using features extracted from demyelinating lesions within the brain parenchyma were developed in the training set. The performance of these models underwent validation within the internal testing set. Additionally, we gathered clinical factors and MRI features of brain parenchymal lesions at their initial presentation. Subsequently, these variables were used in the construction of a clinical prediction model through multivariate logistic regression analysis.

RESULTS: The areas under the curve for the radiomics models (TIWI, T2WI, FLAIR, and the compound model) in the training set were 0.781 (95% CI, 0.689–0.864), 0.959 (95% CI, 0.924–0.987), 0.939 (95% CI, 0.898–0.979), and 0.989 (95% CI, 0.976–0.999), respectively. The areas under the curve for the radiomics models (TIWI, T2WI, FLAIR, and the compound model) in the testing set were 0.500 (95% CI, 0.304–0.652), 0.833 (95% CI, 0.697–0.944), 0.804 (95% CI, 0.664–0.918), and 0.905 (95% CI, 0.803–0.979), respectively. The areas under the curve of the clinical prediction model in the training set and testing set were 0.700 and 0.289, respectively.

CONCLUSIONS: Multiparameter MRI-based radiomics helps distinguish MOGAD from non-MOGAD in patients with idiopathic inflammatory demyelinating diseases.

ABBREVIATIONS: AUC = area under the ROC curve; IIDDs = idiopathic inflammatory demyelinating diseases; LASSO = least absolute shrinkage and selection operator; MOG = myelin oligodendrocyte glycoprotein; MOGAD = myelin oligodendrocyte glycoprotein antibody associated disorders; NMOSD = neuromyelitis optica spectrum disorder; ROC = receiver operating characteristic

Myelin oligodendrocyte glycoprotein antibody-associated disorders (MOGAD) represent a collection of immune-mediated monophasic or multiphasic demyelinating diseases affecting the brain, optic nerve, and spinal cord.¹ This condition

falls under the umbrella of idiopathic inflammatory demyelinating diseases (IIDDs), with the distinguishing feature being the myelin oligodendrocyte glycoprotein (MOG) antibody as a unique biomarker. MOGAD is more prevalent in children than in adults. In children, about 13% of the antibodies that cause autoimmune encephalitis are MOG antibodies.² In contrast, MS occurs less frequently in children than in adults. In children experiencing the initial onset of MOGAD, early diagnosis is of utmost importance. During the acute phase, treatment primarily involves the use of glucocorticoids, high-dose IV immunoglobulin, or plasma exchange. Failure to correctly diagnose MOGAD can result in delayed treatment, progression, and recurrence, ultimately leading to irreversible damage to the CNS following multiple relapses.^{3,4}

The early diagnosis of MOGAD in children continues to pose challenges in both imaging and clinical practice. While the

Received July 6, 2023; accepted after revision September 28.

From the Department of Radiology (T.L., X.C., H.W., T.Z., L.Z., H.D., M.X., L.H.), Children's Hospital of Chongqing Medical University, National Clinical Research Center for Child Health and Disorders Ministry of Education Key Laboratory of Child Development and Disorders, Chongqing Key Laboratory of Pediatrics, Chongqing, China; and Huiying Medical Technology Co (Y.J.), Dongsheng Science and Technology Park, Beijing, China.

Please address correspondence to Ling He, MD, Department of Radiology, Children's Hospital of Chongqing Medical University, National Clinical Research Center for Child Health and Disorders, Ministry of Education Key Laboratory of Child Development and Disorders, Chongqing Key Laboratory of Pediatrics, Chongqing 400014, China, 136 Zhongshan Second Rd, Yuzhong District, Chongqing, China; e-mail: doctorheling@yeah.net

 Indicates article with online supplemental data.

<http://dx.doi.org/10.3174/ajnr.A8045>

detection of MOG antibodies in serum or CSF samples serves as a crucial diagnostic indicator, it typically takes approximately 2 weeks and can be costly. Moreover, some primary hospitals lack the capability to perform such tests, leading to delays in a timely diagnosis.^{5,6} In MOGAD and other IIDDs, brain parenchymal lesions appear as high-signal demyelinating lesions on FLAIR and T2WI sequences. Although previous studies have identified certain MR imaging features associated with brain lesions in children with MOGAD, qualitative MR imaging features are insufficient for identifying these disorders.⁷

In recent years, radiomics has emerged as a novel discipline extensively used in tumor-related diseases. By analyzing the ROI in images, radiomics involves extracting and calculating first-order, second-order, and high-order features. This process enables the discovery of hidden pathology, prognostic indicators, and other features that may not be discernible to the naked eye.⁸ However, the application of radiomics in children with IIDDs has been limited.⁹ Currently, there are no reports on the use of MR imaging radiomics to differentiate IIDDs caused by MOG antibodies and those with other origins. In this study, we aimed to address this gap by constructing models using 3 conventional MRI sequences (T1WI, T2WI, and FLAIR) to distinguish MOGAD from non-MOGAD in patients with IIDDs. The validity and performance of these models were verified and compared, ultimately identifying the model with the most optimal performance. We anticipate that these models will serve as effective tools for computer-aided identification of patients with MOGAD, filling a critical need in the field of IIDDs.

MATERIALS AND METHODS

This retrospective, single-center study was approved by the institutional review board of Children's Hospital of Chongqing Medical University with a waiver of written informed consent.

Patients

We conducted a retrospective collection of clinical and MRI data from children admitted to our neurology department between February 2017 and December 2021. The study focused on children diagnosed with MOGAD and those with other IIDDs during their initial attack.

The inclusion criteria were as follows:

- 1) Acute or subacute onset characterized by single or multiple symptoms such as optic neuritis, encephalitis, meningoencephalitis, brainstem encephalitis, and myelitis.
- 2) Patients with a positive antibody for MOG (excluding other positive antibodies like glial fibrillary acidic protein, *N*-methyl-D-aspartate, and aquaporin-4). Confirmation of negative antibodies to MOG, glial fibrillary acidic protein, *N*-methyl-D-aspartate, and aquaporin-4 was achieved by detecting relevant neurologically autoimmune antibodies in CSF/serum samples using the cell-based assay method.
- 3) Brain MRI examination with clear and complete images showing demyelinating lesions in the brain parenchyma performed within a window of 15 days before or after the neurologically relevant autoimmune antibody test.

Exclusion criteria were as follows:

- 1) The presence of other possible diseases such as neurodegenerative, metabolic, or cerebrovascular.
- 2) Poor image quality that would impede further research.

The flow chart is depicted in the Online Supplemental Data. A total of 121 patients with IIDDs were enrolled in the study, comprising 68 patients with MOGAD and 53 patients without MOGAD. We collected clinical features including sex and age at the time of the initial attack. The study cohort was randomly sampled at a ratio of 7:3 and divided into a training set and a testing set. In the training set, there were 47 patients with MOGAD and 37 patients without MOGAD. The testing set included 21 patients with MOGAD and 16 patients without it.

MR Imaging Technique

The children were examined using a 3T MRI machine (Achieva 3T; Philips Healthcare) or a 1.5T MR imaging machine (Signa Horizon Lx; GE Healthcare). MR images mainly included axial sequences, T1WI (TR = 700 ms, TE = 30 ms), T2WI (TR = 3000 ms, TE = 100 ms), and T2-FLAIR (TR = 8000 ms, TE = 94 ms). Scanning parameters were the following: section number = 16, section thickness = 5 mm, spacing = 1 mm, FOV = 18 × 18 cm, number of excitations = 2–4. Patients who were unable to cooperate were sedated before undergoing MR imaging.

Radiomics Processing

Segmentation of ROIs. The T1WI, T2WI, and FLAIR sequences of brain MRIs from all patients were obtained in DICOM format from the PACS system. The ROI segmentation was performed using ITK-SNAP (Version 3.6.0; www.itksnap.org) software by radiologist 1 with >5 years of diagnostic experience. Radiologist 1 carefully segmented the ROI along the lesion edges on the T1WI, T2WI, and FLAIR images. The ROI encompassed demyelinating lesions in the brain parenchyma and perifocal edema while excluding CSF. Radiologist 2 with 10 years of diagnostic experience verified the segmentation. The agreement of the final selected radiomics features between 2 radiologists was evaluated using intra-class correlation coefficient. The result is depicted in the Online Supplemental Data.

Feature Extraction, Selection, and Model Establishment

Features were extracted from the T1WI, T2WI, and FLAIR sequences of the patient's brain MRIs. The extracted radiomics features encompassed first-order features, shape features, texture features, as well as Laplacian of Gaussian-filtered and wavelet transform features. The selection of radiomics features underwent 4 stages using Python software (PyRadiomics, Version 2.2.0; <https://github.com/AIM-Harvard/pyradiomics/blob/master/docs/index.rst>). In the first stage, features were chosen through variance thresholding, with features having a threshold value of >0.8 retained for further analysis. Subsequently, the features underwent downsampling using the univariate selection method, and features with a *P* value < .05 were retained. Next, the features were selected using a least absolute shrinkage and selection operator (LASSO) regression analysis with 10-fold cross-validation to determine the optimal λ value. Finally, a feature-correlation analysis was performed to select the most relevant features. For each patient, a Radscore was calculated using the

Table 1: Clinical and MR imaging features of patients with and without MOGAD^a

| Patient Characteristic | MOGAD Group | Non-MOGAD Group | P Value |
|--|--------------------|--------------------|---------|
| Age (mean) (median) (yr) | 2.6 [SD, 3.1], 2.6 | 6.5 [SD, 3.7], 6.5 | .045 |
| Sex | | | .217 |
| Male | 27 | 27 | |
| Female | 41 | 26 | |
| Cortex | 22 | 8 | .029 |
| White matter | 54 | 45 | .437 |
| Thalamus | 41 | 17 | .002 |
| Pedunculus cerebri | 23 | 7 | .009 |
| Cerebellar peduncles | 13 | 7 | .385 |
| Multifoci | 66 | 48 | .129 |
| Involvement of both cerebral hemispheres | 57 | 46 | .649 |

^aSignificant difference with *P* value <.05.

Table 2: Univariate and multivariate logistic analysis in the cohort

| Variable | Univariate Analysis (P Value) | Multivariate Analysis (P Value) |
|--|-------------------------------|---------------------------------|
| Age | .041 ^a | .017 ^a |
| Sex | .753 | |
| Cortex | .027 ^a | .021 ^a |
| White matter | .657 | |
| Thalamus | .220 | |
| Pedunculus cerebri | .072 | |
| Cerebellar peduncles | .172 | |
| Multifoci | .116 | |
| Involvement of both cerebral hemispheres | .749 | |

^aSignificant difference with *P* value <.05.

equation, and Radscore models were developed for individual sequences as well as a compound of the 3 sequences.

$$\text{Radscore} = \text{Intercept} + \sum_{i=1}^n \text{coefficients}[i] \times \text{Feature}[i]$$

Patient Characteristics and Clinical Model Building

We collected clinical features including sex and age at the time of the initial attack. Additionally, the MRI presentations of the patient's brain lesions were evaluated, and consensus was reached through discussions by radiologist 1 and radiologist 2. The assessments included the following points: 1) determining the number of lesions (single or multiple); 2) identifying involvement of the cerebral cortex, white matter, thalamus, cerebral peduncle, and cerebellar peduncle; and 3) assessing whether the lesions involved the bilateral cerebral hemispheres. Univariate logistic analysis was performed on the collected clinical and imaging features, and the influencing factors with statistical significance (*P* < .05) were analyzed by multivariate logistic regression analysis to establish the clinical model.

Statistical Analysis

Statistical analysis for this study was conducted using R Studio software (Version 4.1.2; <http://rstudio.org/download/desktop>). Paired-samples *t* tests or nonparametric tests were used for the analysis of clinical and imaging data. To evaluate the efficacy of the models, we used various evaluation metrics, including the receiver operating characteristic (ROC) curve, area under the ROC curve (AUC), accuracy, sensitivity, and specificity, which were assessed

in both the training and testing sets. The DeLong test was applied to compare the effectiveness of different models within the training set. Statistical significance was defined as *P* < .05.

RESULTS

Patient Characteristics and Clinical Model Building

Among the patients with MOGAD, there were 27 males and 41 females, ranging in age from 1 year 7 months to 14 years, with a mean age of 2.6 years. In the non-MOGAD group, there were 27 males and 26 females, ranging from 1 to 13 years of age, with a mean age of 6.5 years. A comparison of the clinical features and MR imaging presentations of the patients is shown in Table 1. The analysis revealed no statistically significant differences in terms of sex, multiple lesions, involvement of lesions in the bilateral cerebral hemispheres, and involvement of the white matter and cerebellar peduncles between the 2 groups (*P* > .05). However, statistically significant differences were observed in

terms of age, involvement of the cortex, thalamus, and pedunculus cerebri (*P* < .05).

Characteristics, including age and involvement of the cortex, were identified as significant with *P* < .05 by univariate analysis. Both of them, age (OR = 1.1896, *P* = .017) and involvement of cortex (OR = 3.9862, *P* = .0207), were selected by multivariate logistic regression analysis (Table 2). The AUCs of the clinical prediction model in the training set and testing set were 0.700 and 0.289. The ROC curves depicting the clinical model are presented in Fig 1.

Feature Extraction and Selection

On the basis of the ROI segmentation performed by 2 radiologists, a total of 1688 features were extracted from the T1WI, T2WI, and FLAIR sequence images. Initially, redundant features were eliminated using the variance threshold method, resulting in the removal of 168, 128, and 127 features with thresholds of <0.8. Subsequently, the single-variable selection method was used, resulting in the selection of 30,233 and 395 features, which were further selected through LASSO regression analysis (Online Supplemental Data). The λ value was determined using 10-fold cross-validation. By applying feature-correlation analysis, a total of 15 features for the T1WI model, 22 features for the T2WI model, 19 features for the FLAIR model, and 32 features for the compound model were selected. The 10 most optimal features for each sequence, used for constructing the radiomics models, are presented in the Online Supplemental Data. By means of the equation, the Radscore was calculated for each patient, and radiomics models were developed for individual sequences as well as the combined analysis of all 3 sequences.

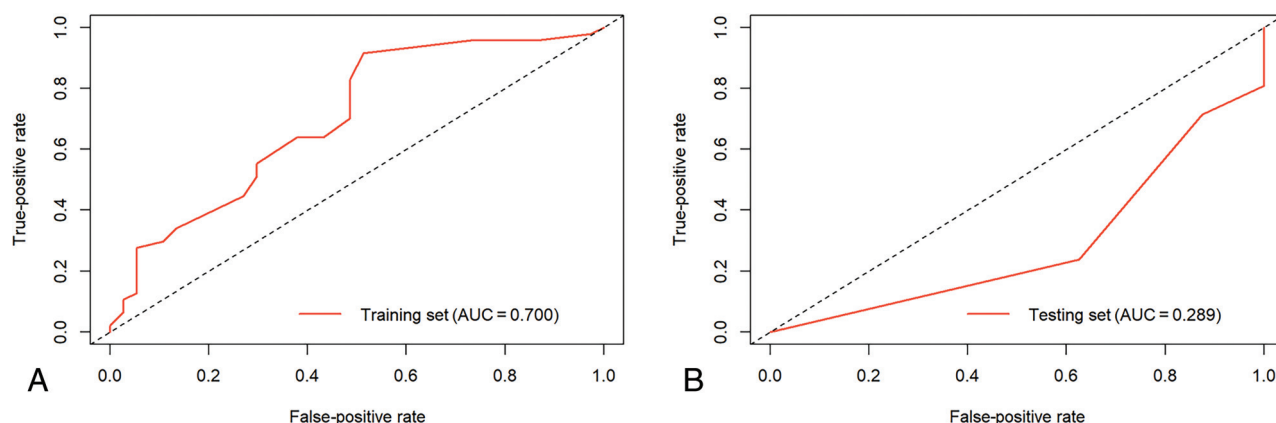


FIG 1. ROC curves of the clinical prediction model in the training and testing sets.

Table 3: Evaluation indexes of T1WI, T2WI, FLAIR, and compound models in the training and testing sets

| Models | AUC (95% CI) | Accuracy | Sensitivity | Specificity |
|--------------|---------------------|----------|-------------|-------------|
| T1WI | | | | |
| Training set | 0.781 (0.689–0.864) | 0.690 | 0.745 | 0.622 |
| Testing set | 0.500 (0.304–0.652) | 0.459 | 0.571 | 0.312 |
| T2WI | | | | |
| Training set | 0.959 (0.924–0.987) | 0.857 | 0.894 | 0.811 |
| Testing set | 0.833 (0.697–0.944) | 0.784 | 0.857 | 0.688 |
| FLAIR | | | | |
| Training set | 0.939 (0.898–0.979) | 0.845 | 0.851 | 0.838 |
| Testing set | 0.804 (0.664–0.918) | 0.730 | 0.762 | 0.688 |
| Compound | | | | |
| Training set | 0.989 (0.976–0.999) | 0.940 | 0.936 | 0.946 |
| Testing set | 0.905 (0.803–0.979) | 0.838 | 0.905 | 0.750 |

Efficacy of Radiomics Models to Identify MOGAD

The T1WI sequence model demonstrated an AUC of 0.781 (95% CI, 0.689–0.864), with accuracy, sensitivity, and specificity values of 69.0%, 74.5%, and 62.2% in the training set, respectively. In the testing set, the values were 0.500 (95% CI, 0.304–0.652) for AUC, 45.9% for accuracy, 57.1% for sensitivity, and 31.2% for specificity.

For the T2WI sequence model, the training set yielded an AUC of 0.959 (95% CI, 0.924–0.987), with accuracy, sensitivity, and specificity values of 85.7%, 89.4%, and 81.1%, respectively. In the testing set, the values were 0.833 (95% CI, 0.697–0.944) for AUC, 78.4% for accuracy, 85.7% for sensitivity, and 68.8% for specificity.

The FLAIR sequence model achieved an AUC of 0.939 (95% CI, 0.898–0.979) in the training set, along with accuracy, sensitivity, and specificity values of 84.5%, 85.1%, and 83.8%, respectively. In the testing set, the values were 0.804 (95% CI, 0.664–0.918) for AUC, 73.0% for accuracy, 76.2% for sensitivity, and 68.8% for specificity.

The compound model combining all 3 sequences had an AUC of 0.989 (95% CI, 0.976–0.999), with accuracy, sensitivity, and specificity values of 94.0%, 93.6%, and 94.6% in the training set, respectively. In the testing set, the values were 0.905 (95% CI, 0.803–0.979) for AUC, 83.8% for accuracy, 90.5% for sensitivity, and 75.0% for specificity (Table 3). The ROC curves depicting the models are shown in Fig 2.

The DeLong test indicated that the efficacy of the compound model, as well as the FLAIR and T2WI sequence models, was

superior to that of the T1WI model, with statistically significant differences. Additionally, the compound model showed higher efficacy than the FLAIR sequence model, while the differences between the compound model and the T2WI sequence model, as well as between the FLAIR sequence model and the T2WI sequence model, were not statistically significant (Table 4).

DISCUSSION

Although MOGAD was introduced as a new subtype of IIDD in 2018, our understanding of this condition has improved with time, revealing that the MOG antibody is the most common autoimmune antibody associated with IIDDs in children.¹⁰ MR imaging plays a crucial role in the clinical assessment of patients with MOGAD. In MOGAD, brain parenchymal lesions appear as high-signal demyelinating lesions in FLAIR and T2WI sequences.¹¹ These lesions resemble those seen in acute disseminated encephalomyelitis and typically manifest as asymmetrically distributed multiple lesions with indistinct borders, potentially accompanied by edema around larger lesions. MR imaging offers high soft-tissue resolution, multiple parameters, and diverse sequences, enabling the visualization of demyelinating lesions in IIDDs.¹²

Although previous studies have identified certain MR imaging features associated with brain lesions in children with MOGAD such as a higher involvement of the cortex, thalamus, and cerebral peduncle compared with those without MOGAD, these manifestations lack specificity, and accurate diagnosis cannot rely solely on imaging features.¹³ As in the clinical model based on

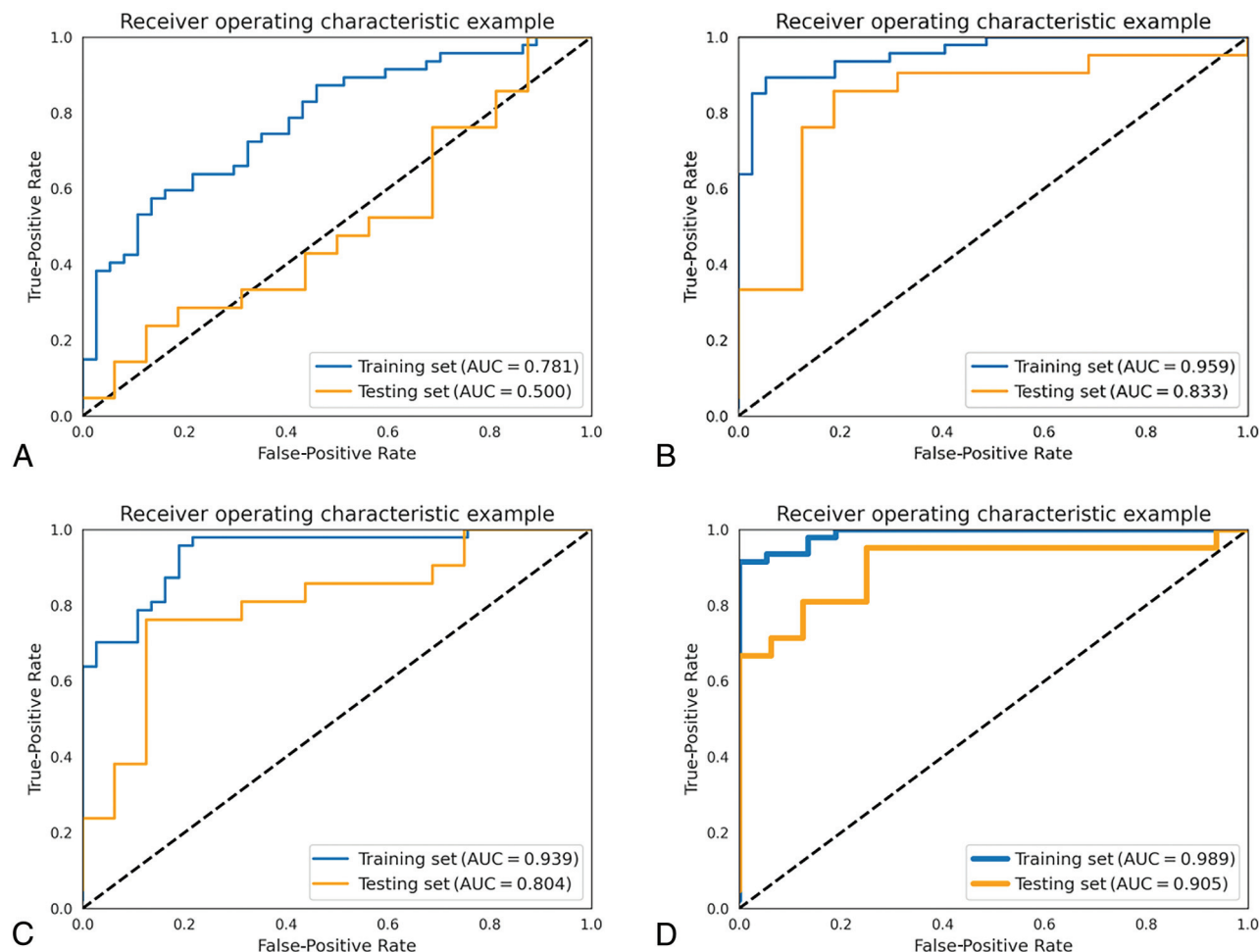


FIG 2. ROC curves of the radiomics models. TIWI (A), T2WI (B), FLAIR (C), and the compound model (D) of 3 sequences.

Table 4: DeLong test among TIWI, T2WI, FLAIR, and compound models in the training set

| Models | | DeLong Test (P value) |
|-----------------------|-----------------------|-----------------------|
| TIWI training set | T2WI training set | 0.0018 |
| | FLAIR training set | 0.0041 |
| T2WI training set | FLAIR training set | 0.3317 |
| | Compound training set | 0.0502 |
| FLAIR training set | Compound training set | 0.0061 |
| Compound training set | TIWI training set | <0.0001 |

clinical and imaging features in this study, efficacy was low in both the training and testing groups. The AUCs of the clinical prediction model in the training set and testing set were 0.700 and 0.289. The emergence of radiomics, a field that uses automated data-mining algorithms to extract high-throughput, non-visualized feature parameters from images, has shown great potential in elucidating the pathology, efficacy, and prognosis of various lesions.¹⁴ While radiomics is predominantly used in tumor-related diseases, its application in IIDDs in children, particularly using MR imaging radiomics, remains unexplored.

To date, only a limited number of studies have investigated the application of MR imaging radiomics in IIDDs, particularly in MS. These studies have demonstrated the potential of MR

imaging radiomics in the diagnosis and prediction of MS progression.⁹ For instance, research has shown that radiomics based on T2WI sequences in brain MRIs can effectively differentiate MS from central small-vessel disease.¹⁵ Moreover, a compound MR imaging model using T1WI and T2WI sequences has been shown to successfully distinguish white matter lesions between MS and neuromyelitis optica spectrum disorder (NMOSD).¹⁶ Furthermore, MR imaging radiomics has proved effective in predicting the progression of MS, with certain studies establishing models based on the T2WI sequence to predict the progression of unenhanced MS lesions.¹⁷ Existing MR imaging radiomics studies in MS have predominantly focused on a single sequence or compound modeling of 2 sequences, leading to a biased selection. Due to the absence of standardized criteria for sequence selection, choosing the most appropriate MRI sequence for radiomics modeling can effectively enhance diagnostic performance.¹⁸

This study used the imaging data from our center to extract features from 3 conventional MR imaging sequences, enabling the establishment of robust radiomics models for differentiating MOGAD and non-MOGAD. Most interesting, 2 of the most crucial features identified in previous MRI-based radiomics research to differentiate MS from NMOSD were texture

features.¹⁹ In our prediction models, a large portion of the 4 models comprised texture features. Previous reports have indicated that texture heterogeneity is associated with the severity of histopathologic injury.²⁰ Another MRI-based radiomics discrimination study between MS and NMOSD discovered differences in Gln values within the gray-level run length matrix features of patients with MS and NMOSD. It potentially reflecting varying degrees of tissue damage between the 2 conditions.²¹ Gln measures the similarity of gray level values throughout the ROI. If the gray level values are similar, the value is small. In our study, the gray-level run length matrix is included within the texture features of the models, suggesting the presence of differences in tissue damage between MOGAD and non-MOGAD. Additionally, some valuable features extracted in this study were derived from wavelet transform. Wavelet transform encompasses intensity and texture information and applies a linear or radial wave matrix to the image. It can capture the spatial relationship among ≥ 3 pixels, potentially uncovering more nuanced information regarding the pathologic level of the lesions. However, further research is necessary to confirm these findings.

Moreover, while most radiomics studies on MS primarily use T2WI sequences, our study demonstrates that both T2WI and FLAIR models have excellent performance. The classification efficiency of the T2WI and FLAIR sequence models is significantly superior to that of the T1WI sequence model. This heightened classification efficiency in the T2WI and FLAIR sequence models may stem from the higher ability to distinguish demyelinating lesions. Additionally, it is possible that the features extracted from T2WI and FLAIR sequences more effectively capture the underlying pathology of demyelinating lesions. Notably, in this study, the compound model that combines features from all 3 sequences demonstrates higher diagnostic efficiency compared with the single-sequence models of T1WI and FLAIR.

However, this study has several limitations. First, it is a retrospective study, which may introduce selection bias and limit the generalizability of the findings. Therefore, further confirmation of these results is warranted through prospective studies. Second, the present study used only conventional sequences of brain MRIs for modeling purposes. In future investigations, incorporating additional imaging techniques such as quantitative MRI and fMRI features could potentially enhance the efficiency of our radiomics model. Previous studies have shown that incorporating magnetization transfer imaging features from quantitative MRI can improve the performance of models in identifying MS.²² Third, the original image-layer thickness in this study was 5 mm, and although the spatial resolution was improved to 1 mm during preprocessing, the improvement may have resulted in lower accuracy in delineating boundaries of small lesions. Therefore, the 5-mm image-layer thickness was used in this study, but this might have an impact on the diagnostic performance of radiomic features. Last, the sample size in this study is relatively small. MOGAD is a newly proposed subtype of IIDDs, and previous cases are limited. Hence, in future studies, a multicenter prospective design should be established to expand the sample size and further validate the findings.

CONCLUSIONS

In this study, we have demonstrated that radiomics models based on T2WI, FLAIR sequences, and a compound model of 3 conventional sequences in brain MR imaging can effectively and early on distinguish children with unknown causes of IIDDs during their initial onset. We have also identified the important role of textural features in the differential diagnosis. Notably, both the T2WI and FLAIR models exhibited exceptional performance as single-sequence models. Moreover, the compound model showed superior diagnostic capability compared with the T1WI and FLAIR models individually, thereby addressing the gap in radiomics application for IIDDs beyond MS. We believe that radiomics holds great potential for extension to other subtypes of IIDDs in the future and will find widespread use in the diagnosis, evaluation, and prognosis of demyelinating diseases in children.

Disclosure forms provided by the authors are available with the full text and PDF of this article at www.ajnr.org.

REFERENCES

- Wynford-Thomas R, Jacob A, Tomassini V. **Neurological update: MOG antibody disease.** *J Neurol* 2019;266:1280–86 [CrossRef Medline](#)
- Jarius S, Ruprecht K, Kleiter I, et al; in cooperation with the Neuromyelitis Optica Study Group (NEMOS). **MOG-IgG in NMO and related disorders: a multicenter study of 50 patients. Part 2: Epidemiology, clinical presentation, radiological and laboratory features, treatment responses, and long-term outcome.** *J Neuroinflammation* 2016;13:280 [CrossRef Medline](#)
- Bruijstens AL, Lechner C, Flet-Berliac L, et al; E.U. Paediatric MOG Consortium. **E.U. Paediatric MOG Consortium consensus, Part 1: classification of clinical phenotypes of paediatric myelin oligodendrocyte glycoprotein antibody-associated disorders.** *Eur J Paediatr Neurol* 2020;29:2–13 [CrossRef Medline](#)
- Armangue T, Olive-Cirera G, Martinez-Hernandez E, et al; Spanish Pediatric anti-MOG Study Group. **Associations of paediatric demyelinating and encephalitic syndromes with myelin oligodendrocyte glycoprotein antibodies: a multicentre observational study.** *Lancet Neurol* 2020;19:234–46 [CrossRef Medline](#)
- Narayan R, Simpson A, Fritsche K, et al. **MOG antibody disease: a review of MOG antibody seropositive neuromyelitis optica spectrum disorder.** *Mult Scler Relat Disord* 2018;25:66–72 [CrossRef Medline](#)
- Hennes EM, Baumann M, Lechner C, et al. **MOG spectrum disorders and role of MOG-antibodies in clinical practice.** *Neuropediatrics* 2018;49:3–11 [CrossRef Medline](#)
- Baumann M, Grams A, Djurdjevic T, et al. **MRI of the first event in pediatric acquired demyelinating syndromes with antibodies to myelin oligodendrocyte glycoprotein.** *J Neurol* 2018;265:845–55 [CrossRef Medline](#)
- Mayerhoefer ME, Materka A, Langs G, et al. **Introduction to radiomics.** *J Nucl Med* 2020;61:488–95 [CrossRef Medline](#)
- Eichinger P, Zimmer C, Wiestler B. **AI in radiology: where are we today in multiple sclerosis imaging?** *Rofo* 2020;192:847–53 [CrossRef Medline](#)
- Fernandez-Carbonell C, Vargas-Lowy D, Musallam A, et al. **Clinical and MRI phenotype of children with MOG antibodies.** *Mult Scler* 2016;22:174–84 [CrossRef Medline](#)
- Mao L, Yang L, Kessi M, et al. **Myelin oligodendrocyte glycoprotein (MOG) antibody diseases in children in central south China: clinical features, treatments, influencing factors, and outcomes.** *Front Neurol* 2019;10:868 [CrossRef Medline](#)
- Borisov N, Mori M, Kuwabara S, et al. **Diagnosis and treatment of NMO spectrum disorder and MOG-encephalomyelitis.** *Front Neurol* 2018;9:888 [CrossRef Medline](#)

13. Cross H, Sabiq F, Ackermans N, et al. **Myelin oligodendrocyte glycoprotein (MOG) antibody positive patients in a multi-ethnic Canadian cohort.** *Front Neurol* 2020;11:525933 [CrossRef Medline](#)
14. Fornaçon-Wood I, Faivre-Finn C, O'Connor JP, et al. **Radiomics as a personalized medicine tool in lung cancer: separating the hope from the hype.** *Lung Cancer* 2020;146:197–208 [CrossRef Medline](#)
15. He T, Zhao W, Mao Y, et al. **MS or not MS: T2-weighted imaging (T2WI)-based radiomic findings distinguish MS from its mimics.** *Mult Scler Relat Disord* 2022;61:103756 [CrossRef Medline](#)
16. Huang J, Xin B, Wang X, et al. **Multi-parametric MRI phenotype with trustworthy machine learning for differentiating CNS demyelinating diseases.** *J Transl Med* 2021;19:377 [CrossRef Medline](#)
17. Peng Y, Zheng Y, Tan Z, et al. **Prediction of unenhanced lesion evolution in multiple sclerosis using radiomics-based models: a machine learning approach.** *Mult Scler Relat Disord* 2021;53:102989 [CrossRef Medline](#)
18. Kang D, Park JE, Kim YH, et al. **Diffusion radiomics as a diagnostic model for atypical manifestation of primary central nervous system lymphoma: development and multicenter external validation.** *Neuro Oncol* 2018;20:1251–61 [CrossRef Medline](#)
19. Bathla G, Priya S, Liu Y, et al. **Radiomics-based differentiation between glioblastoma and primary central nervous system lymphoma: a comparison of diagnostic performance across different MRI sequences and machine learning techniques.** *Eur Radiol* 2021;31:8703–13 [CrossRef Medline](#)
20. Huh SY, Min JH, Kim W, et al. **The usefulness of brain MRI at onset in the differentiation of multiple sclerosis and seropositive neuromyelitis optica spectrum disorders.** *Mult Scler* 2014;20:695–704 [CrossRef Medline](#)
21. Ma X, Zhang L, Huang D, et al. **Quantitative radiomic biomarkers for discrimination between neuromyelitis optica spectrum disorder and multiple sclerosis.** *J Magn Reson Imaging* 2019;49:1113–21 [CrossRef Medline](#)
22. Lavrova E, Lommers E, Woodruff HC, et al. **Exploratory radiomic analysis of conventional vs. quantitative brain MRI: toward automatic diagnosis of early multiple sclerosis.** *Front Neurosci* 2021;15:679941 [CrossRef Medline](#)